



Contents lists available at SciVerse ScienceDirect

Journal of Sound and Vibration

journal homepage: www.elsevier.com/locate/jsv

Novel active and passive anti-vibration mountings

M. Moshrefi-Torbati^{a,*}, J.A. Forrester^a, A.I.J. Forrester^b, A.J. Keane^b,
M.J. Brennan^c, S.J. Elliott^d^a Research Institute for Industry, University of Southampton (UoS), Southampton SO17 1BJ, UK^b Computational Engineering and Design Group, University of Southampton (UoS), Southampton SO17 1BJ, UK^c Department of Mechanical Engineering, UNESP, Ilha Solteira, SP 15385-000, Brazil^d Institute of Sound & Vibration Research, University of Southampton (UoS), Southampton SO17 1BJ, UK

ARTICLE INFO

Article history:

Received 7 April 2011

Received in revised form

22 November 2011

Accepted 2 December 2011

Handling Editor: D.J. Wagg

Available online 21 December 2011

ABSTRACT

This paper investigates a novel design approach for a vibration isolator for use in space structures. The approach used can particularly be applicable for aerospace structures that support high precision instrumentation such as satellite payloads. The isolator is a space-frame structure that is folded in on itself to act as a mechanical filter over a defined frequency range. The absence of viscoelastic elements in such a mounting makes the design suitable for use in a vacuum and in high temperature or harsh environments with no risk of drift in alignment of the structure. The design uses a genetic algorithm based geometric optimisation routine to maximise passive vibration isolation, and this is hybridised with a geometric feasibility search. To complement the passive isolation system, an active system is incorporated in the design to add damping. Experimental work to validate the feasibility of the approach is also presented, with the active/passive structure achieving transmissibility of about 19 dB over a range of 1–250 Hz. It is shown here that the use of these novel anti-vibration mountings has no or little consequent weight and cost penalties whilst maintaining their effectiveness with the vibration levels. The approach should pave the way for the design of anti-vibration mountings that can be used between most pieces of equipment and their supporting structure.

Crown Copyright © 2011 Published by Elsevier Ltd. All rights reserved.

1. Introduction

For space launch vehicles, it is essential to isolate the vibration of aerospace structures to prevent damage to the payload. Vibrations have long been a source of problems for space systems, where in addition to failure during launch, periodic disturbances have also degraded their on-orbit performances. As well as increased launch survivability, reducing vibration during the launch may also allow the design of more sensitive instruments with improved on-orbit performance [1].

Commonly, the solution to the vibration isolation problem is to use anti-vibration mounts or viscoelastic coatings on structural elements to enhance the damping [2]. These solutions lead to weight and cost penalties and the effectiveness of such measures diminishes with increasing levels of vibration, making increasingly stringent noise and vibration targets

* Corresponding author. Tel.: +44 2380598583; fax: +44 2380597051.

E-mail addresses: m.m.torbati@soton.ac.uk (M. Moshrefi-Torbati), jennifer.forrester@soton.ac.uk (J.A. Forrester), Alexander.Forrester@soton.ac.uk (A.I.J. Forrester), Andy.Keane@soton.ac.uk (A.J. Keane), mjbrennan0@btinternet.com (M.J. Brennan), S.J.Elliott@soton.ac.uk (S.J. Elliott).

more difficult to meet [3]. The damping materials are also unable to maintain their properties in harsh environments due to their temperature dependence, making them impractical for space applications.

In recent years a number of active and passive vibration isolation solutions have been proposed and tested [4]. Some of the more successful solutions include Hexapod or Stewart Platforms, dual-chamber pneumatic springs, passive D-strut systems, zero-spring-rate mechanisms, voice coil actuators, open/closed cell foam designs, smart structures and shape memory alloy isolators. Perhaps, one of the most effective designs has been the SoftRide MultiFlex whole-spacecraft vibration isolation system which consists of a series of identical isolator elements [5]. This system has proved to be a very effective means of reducing spacecraft response due to broadband structure-borne launch vibration and the low-frequency launch loads. Further improvements have been obtained by employing a multi-axis system, which inserts flexibility and damping in three orthogonal axes between the launch vehicle and the satellite.

An alternative approach to the above-mentioned methods is to design structures with inherent vibration isolation properties. Therefore, a generic structural design capability is required through which beneficial vibration characteristics can be built into structures, whilst their ability to achieve highly accurate measurements or alignment is retained, along with their static load carrying capacity [6].

A previous study by some of the authors of this paper [7], has demonstrated that a genetic algorithm (GA) based geometric optimisation routine can be used to produce a space-frame structure with the desired characteristics within a given frequency range. As with vibration isolators that are currently used, the resulting optimised structure constrained the vibrational energy close to the point of excitation, reducing the need for additional damping treatment and allowing any treatments to be concentrated in regions of where they are most effective. The structure was optimised based on energy flow analysis models and relied on the wavelengths of the vibrations of interest being of a similar order to the changes introduced into the geometry of the structure during optimisation [8]. Because of this limitation, an active control system was used to control the lower frequency vibration. In practice, the passive response of such structures can be optimised for the higher frequency ranges that are of particular interest for sensitive equipment requiring a high-degree of pointing accuracy.

Following on from this work, the present study investigates the use of a *folded* space-frame structure as an anti-vibration mounting. The computational design of a passive structure [9] is combined with co-located ‘sky-hook’ damping [10] into a compact vibration isolation mount with improved ease of assembly [11]. The design is tested dynamically to demonstrate the significant attenuation afforded by the combined passive and active elements. This novel concept may represent a new type of lightweight and cost effective anti-vibration mounting designs.

The first part of the work is concerned with the study of small-scale folded optimised structures and their vibration reduction characteristics. The primary question of interest is whether the desirable vibration filtering characteristics that have been engineered into an unfolded boom-type structure in the previous study can be realised in a folded structure, given the severe restrictions inherent in the layout and manufacture of such devices. The principal difficulty is in controlling the design process so that good isolation can be achieved whilst producing designs that can be physically realised and manufactured. Section 2 describes the process of constructing a folded structure and calculating a measure of its physical feasibility that can be used as an optimisation cost function. Section 3 details the integration of a feasibility search into a GA search for optimum vibration isolation. The design of the Skyhook active vibration control is described in Section 4 and testing of a prototype structure and results are discussed in Section 5 before conclusions are drawn in Section 6.

2. Isolator construction method

The novel metallic isolators, shown in Figs. 1 and 2, were constructed using a series of rods connected at joints. Each joint (except for the base and mounting end) has six rods attached to it and the existence of acute angles between these rods implies that they begin to intersect each other well away from the joints. Due to the number of alternative structures planned for testing, a generic method of joining the rods was required, thereby significantly reducing cost by re-use and by eliminating the need for bespoke joints at each intersection. To overcome the problem due to acute angles, the rod ends were shifted slightly away from the centre of the joint via a re-usable generic joint design, which is shown in Fig. 3.

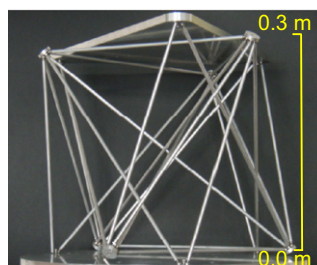


Fig. 1. Regular 3-bay structure.

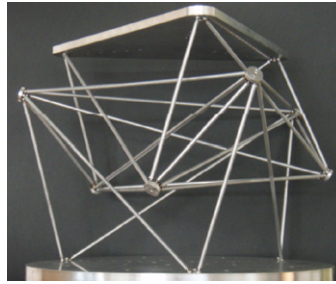


Fig. 2. Irregular optimised 3-bay structure.

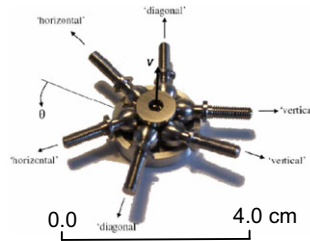


Fig. 3. Generic ball joint.

Each of the rods, all with different lengths, contains a screw thread to which a ball-end was attached. The ball-ends were located in a race which was clamped when the structure was assembled. Each joint could accommodate angles between the rods of 0° to 180° . From the Chebychev–Grübler–Kutzbach's formulae [12], an assembly of three bays is in fact a mechanism with 42 degrees of freedom. Whilst in a support fixture, seven or more accessible ball joints need to be tungsten inert gas (TIG) welded to a neighbouring joint to create a structure. The second issue for construction was that, even for a three-bay design, the chance of rods intersecting each other elsewhere was increased by extending each bay back into the structure. Any slight shift in the joint positions was likely to cause the rods to intersect each other. This complex problem, compounded by the ball-jointed geometry, is discussed below.

The prototype structures shown in Figs. 1 and 2 had a mean bay length of 0.3 m. This scale of structure facilitated the manufacture and test of the concept. It is envisaged that scaled down versions could be used in satellite applications, but would require more advanced manufacturing, such as lost wax or selective laser sintering processes.

2.1. Geometry feasibility

Many possible folded structures will suffer from intersections of various elements and this problem increases as the number of bays is increased. The Monte-Carlo simulations, using the analysis detailed below, have shown that only 0.8% of three-bay and fewer than 0.02% of five-bay geometries are feasible. Therefore, a systematic way of identifying feasible designs is needed. In the approach adapted here, initially the joints are oriented such that v in Fig. 3 is aligned with the average angle of the rods emanating from the joints. Having positioned the joint, each ball-end is allocated a position in the race. The two rods making up the triangles between each bay are positioned together with the 'diagonal' rods either side. The two remaining rods that connect between bays are allocated the final two slots. Checks are made on the intersections in these connecting rods and their positions switched if required. Having constructed the initial geometry, the algorithm must now work through all possible rod pairs checking for other intersections. Intersections in the geometry are found by first calculating if two rods, defined as lines with ends given by the vectors \mathbf{x}_1 , \mathbf{x}_2 and \mathbf{x}_3 , \mathbf{x}_4 are in the same plane, i.e., if:

$$(\mathbf{x}_1 - \mathbf{x}_3) \cdot [(\mathbf{x}_2 - \mathbf{x}_1) \times (\mathbf{x}_4 - \mathbf{x}_3)] = 0 \quad (1)$$

If so, and the lines are not parallel, then the point of intersection is calculated by

$$\mathbf{x} = \mathbf{x}_1 + (\mathbf{x}_2 - \mathbf{x}_1) \frac{[(\mathbf{x}_3 - \mathbf{x}_1) \times (\mathbf{x}_4 - \mathbf{x}_3)] \cdot [(\mathbf{x}_2 - \mathbf{x}_1) \times (\mathbf{x}_4 - \mathbf{x}_3)]}{|(\mathbf{x}_2 - \mathbf{x}_1) \times (\mathbf{x}_4 - \mathbf{x}_3)|^2} \quad (2)$$

If, as in most cases, the rods are not coplanar, the minimum distance between a pair of skew lines is given by

$$\varepsilon = \frac{|(\mathbf{x}_3 - \mathbf{x}_1) \cdot [(\mathbf{x}_2 - \mathbf{x}_1) \times (\mathbf{x}_4 - \mathbf{x}_3)]|}{|(\mathbf{x}_2 - \mathbf{x}_1) \times (\mathbf{x}_4 - \mathbf{x}_3)|} \quad (3)$$

This distance is along the vector

$$\mathbf{v} = \frac{[(\mathbf{x}_2 - \mathbf{x}_1) \times (\mathbf{x}_4 - \mathbf{x}_3)]}{|(\mathbf{x}_2 - \mathbf{x}_1) \times (\mathbf{x}_4 - \mathbf{x}_3)|} \quad (4)$$

To find the minimum distance, \mathbf{x}_3 and \mathbf{x}_4 are transformed to \mathbf{x}'_3 and \mathbf{x}'_4 along vector \mathbf{v} by the distance ε . The minimum distance is the point of intersection of the lines \mathbf{x}_1 , \mathbf{x}_2 and \mathbf{x}'_3 and \mathbf{x}'_4 . If the lines are in the same plane and intersecting or the distance ε is less than the rod diameter (plus a tolerance) and the point of minimum distance satisfies

$$\min\{x_1(1), x_2(1), x'_3(1), x'_4(1)\} < x < \max\{x_1(1), x_2(1), x'_3(1), x'_4(1)\} \quad (5)$$

then an intersection has occurred. The whole structure is considered finding ε for each pair of rods and then the feasibility function is calculated by

$$\varepsilon = \sum_j \sum_i (-\varepsilon_{ij}) \quad (6)$$

where ε_{ij} is the distance between the centrelines of rods i and j , calculated using Eq. (3), and ε is the distance aimed for the diameter plus a tolerance (here a tolerance of 2.5 mm is used, i.e., the rods should be at least 2.5 mm apart). When $\varepsilon=0$ there is a feasible geometry.

When searching for optimal geometries it is inevitable that infeasible structures will be created. Having found an infeasible geometry, two options are available: the geometry can be discarded and optimisation techniques capable of dealing with 'missing data' can be used, or the geometry can be repaired by perturbing the joints until the closest possible feasible structure is found. Both approaches were considered during this study with the second option, detailed in the next section, chosen as the most suitable approach.

3. Passive structure design methodology

Having determined a method of manufacture and the constraints that would need to be incorporated in the optimisation routine to allow manufacture, a regular design could be implemented. The theoretically feasible optimisation routine could then be used to design an irregular structure. The designs use three 'bays', with each of the bays in the irregular structure acting as a filter for a certain frequency range. The aim of the computational analysis was to design a structure that minimises vibration at three equipment mounting points when subjected to a unit harmonic force at three points on the base across a frequency range of 150–250 Hz.

Two analysis codes were considered: finite element analysis with one-dimensional Euler–Bernoulli beam elements with artificially stiff elements to represent the joints (run time, order 5 min) and a receptance theory based code with point masses at the joints (run time order 10 s). The results of each were compared using the regular structure and showed a clear trade-off between speed and accuracy. Given that the expectation was to perform over 10,000 structure evaluations the most practical code to use was the receptance code. Based on the above run times, the GA ~28 CPU hours using the receptance code vs. ~35 CPU days using FEA. This does not include geometry repair time, with each repair dependent on the starting geometry, though roughly equivalent to the receptance code run time. The number of repairs is in turn dependent on the initial GA population.

To minimise the sensitivity to minor geometric changes, the performance of the structure was measured by observing the vibration energy in the connecting rods at the three joints of interest. The objective function for the optimisation was a function of the beam kinetic energies with values taken and averaged at a number of points over the frequency range selected to minimise computation time whilst avoiding aliasing. It was likely that the objective function would behave in a highly multi-modal manner as joint positions were varied. In order to ensure that the optimisation algorithm did not become trapped in local minima, a global optimisation algorithm was chosen that could be integrated with the approach to infeasible designs (i.e., a genetic algorithm).

Due to the high level of infeasibility (99.2% for the 3-bay structure based on 1000 randomly generated designs) rejecting infeasible designs in the initiation of the algorithm results in loss of population diversity and the risk of convergence towards a local optimum. Therefore, a Darwinian–Lamarckian hybrid approach [13] was taken to 'repair' infeasible geometries when discovered throughout the routine using a gradient-based sequential quadratic programming (SQP) search of an algorithmically differentiated implementation of the feasibility metric Eq. (6) [14].

The Matlab function for calculating the feasibility function was differentiated with respect to the design variables (the x, y, z locations of the joints) using the MAD toolbox [15]. Occasionally, a feasible design will still not be found, but the number of these occurrences decays gradually through the generations of the GA. The best geometry after 100 generations gave a 15 dB reduction in energy compared with the regular structure. Fig. 4 shows the progress of this GA while Fig. 5 shows the diminishing level of infeasibility due to the Lamarckian learning element of the search (the gradient-based geometry repair). Physical testing of the optimised structure in Fig. 2 is discussed in Section 5.

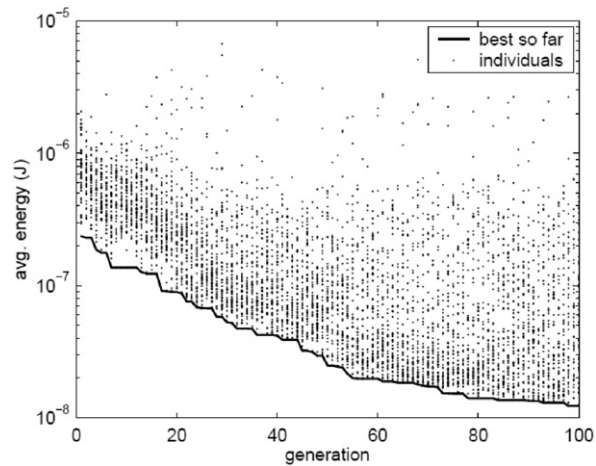


Fig. 4. Progress of the hybrid optimisation.

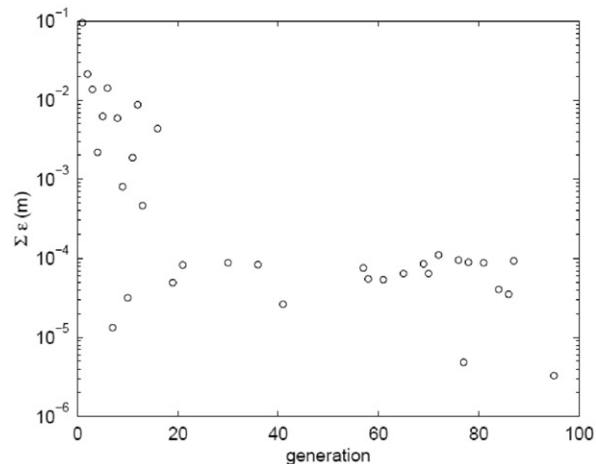


Fig. 5. Level of geometry infeasibility throughout the hybrid optimisation.

4. Active element design methodology

Passive vibration isolation systems, such as those using the isolator described above, are designed to have light damping to provide good isolation at frequencies well above the fundamental resonance frequency. Significant damping is, however, required to suppress the response at the fundamental resonance frequency, resulting in a trade-off in performance at different frequency levels. This inherent compromise can be avoided by implementing an active system with velocity feedback control. Conventional methods of modelling vibration isolators usually assume that the isolator is mass-less. Typically, this assumption will tend to overestimate performance due to neglected internal resonances (IR), or wave effects in the isolator [16]. This overestimation is particularly pertinent in this study because the structure could form a significant proportion of the total mass of the arrangement and lightly damped metallic isolators have smaller loss factors resulting in more significant wave effects. In this section, an analytical model, developed in Ref. [10] which is based on absolute velocity feedback (AVF) control is adopted by considering the mount as a continuous rod and using mobility and impedance methods to assess the adapted approach.

It should be stressed that employing AVF to attenuate vibration over the given frequency range would imply that external power is needed to achieve the improved performance. This may introduce a feasibility issue, particularly with using the proposed design in space systems. However, this requirement should be judged against the additional incurred weight penalties, when other passive damping solutions, such as viscoelastic damping, are used or higher external power requirements when other existing anti-vibrations mounts, such as a Stewart Platform or a whole-spacecraft vibration isolation system, are employed.

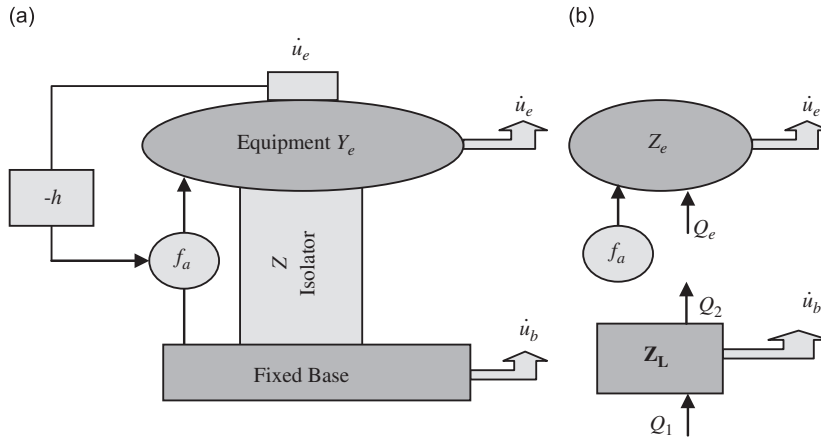


Fig. 6. (a) Schematic diagram and (b) free body diagram of base excited active vibration isolation system containing a distributed parameter isolator under AVF control, where \dot{u}_e and \dot{u}_b are velocities of the equipment and the base respectively; Z_e is the input impedance of the unconnected equipment at the location of the isolator connection; Z_L is the impedance matrix of the isolator; h is the constant feedback control gain; f_a is the active control force; and Q_e, Q_1 and Q_2 are internal forces.

4.1. Performance of Absolute Velocity Feedback (AVF) control

Fig. 6 shows a base excited active vibration isolation system consisting of an isolated equipment represented by its impedance Z_e supported by a distributed parameter isolator under AVF control.

For simplicity, to demonstrate the effectiveness of AVF control the isolator is here modelled as a finite elastic rod. The control force f_a , which is in parallel with the isolator, acts between the equipment and the base. The control force is given by $f_a = -h\dot{u}_e$ which is proportional to the velocity of the equipment that is fed back to the system through a feedback controller with a constant gain $-h$. The dynamics of the system in Fig. 6 are described as follows [10]:

$$Q_e = -Q_2 = Z_e \dot{u}_e$$

$$\begin{bmatrix} Q_1 \\ Q_2 \end{bmatrix} = Z_L \begin{bmatrix} \dot{u}_b \\ \dot{u}_e \end{bmatrix} = \begin{bmatrix} Z_{11} & Z_{12} \\ Z_{21} & Z_{22} \end{bmatrix} \begin{bmatrix} \dot{u}_b \\ \dot{u}_e \end{bmatrix} \quad (7)$$

and

$$Z_e \dot{u}_e = f_a + Q_e = f_a - Q_2 \quad (8)$$

The velocity of the equipment is therefore given by

$$\dot{u}_e = \frac{1}{Z_e + Z_{22}} f_a + \frac{-Z_{21}}{Z_e + Z_{22}} \dot{u}_b \quad (9)$$

Substituting f_a into Eq. (9), gives the transmissibility, T , of the system under AVF control

$$T = \frac{\dot{u}_e}{\dot{u}_b} = \frac{-Z_{21}}{Z_e + Z_{22} + h} \quad (10)$$

If the equipment is modelled as a mass (i.e., $Z_e = j\omega m_e$), the transmissibility can be written in the following non-dimensional form:

$$T = \frac{1}{\cos[\sqrt{\mu_i}(1-j(\eta_i/2))\Omega] - ((\Omega - j2\zeta_a)/(\sqrt{\mu_i}))(1-j(\eta_i/2))\sin[\sqrt{\mu_i}(1-j(\eta_i/2))\Omega]} \quad (11)$$

where $\zeta_a = 1/2h(K_L m_e)^{-1/2}$ is the active damping ratio due to AVF control in which K_L is the static longitudinal stiffness of the isolator, m_e is the mass of an additional SDOF system; μ_i is the mass or rotational inertia ratio of the isolator to that of the equipment; η_i is the loss factor in a distributed parameter isolator; Ω is the ratio of the excitation frequency ω , to the system fundamental natural frequency $\omega_e = K_L^{1/2} m_e^{-1/2}$.

The role of AVF for the base excited system containing a distributed parameter isolator appears to be the same as a skyhook damper [17], adding a damping term to the denominator of Eq. (11). This is further demonstrated in Fig. 7 where AVF control in the base excited system is shown to be equivalent to a viscous damper with damping coefficient h acting between the equipment and the inertial ground.

The transmissibility for this active vibration isolation system with different values of active damping ratio is plotted in Fig. 8.

It can be seen that the system's fundamental resonance peak is attenuated when the active damping ratio is increased. However, little reduction at the IR peaks in the distributed parameter isolator is achieved by AVF control. Since, the feedback controller has a constant gain, the stability of the AVF control system can be analysed by investigating the

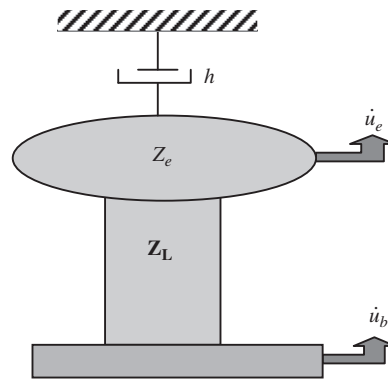


Fig. 7. Mechanical passive representation of the base excited active vibration isolation system containing a distributed parameter isolator under AVF control.

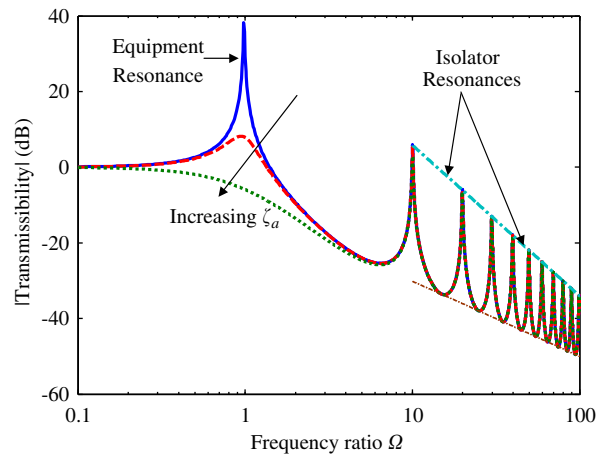


Fig. 8. Transmissibility of the active vibration isolation system under AVF control when the ratio of the mass of the isolator to the mass of the equipment is $\mu_i=0.1$, the loss factor in the isolator is $\eta_i=0.01$ and the active damping ratio is $\zeta_a=0$ (solid line), $\zeta_a=0.2$ (dashed line) and $\zeta_a=1.0$ (dotted line). The bold and faint dashed-dotted lines pass through the IR peaks and the troughs of the transmissibility, respectively.

response of the system with unit control gain of $h=1$. From Eq. (9), the plant response due to the active control force is given by

$$G = \left. \frac{\dot{u}_e}{f_a} \right|_{\dot{u}_b=0} = \frac{1}{Z_e + Z_{22}} \quad (12)$$

Since Z_e and Z_{22} are both point impedances, their phase is between -90° and 90° and hence the overall phase shift of the plant response is completely passive and between -90° and 90° . The Nyquist plot for this system is entirely on the right-hand side of the complex plane [16]. The feedback system has an infinite gain margin and a phase margin of at least 90° . Based on the Nyquist criterion, this AVF control system containing a distributed parameter isolator under base motion is unconditionally stable.

5. Testing and validation of results

Having constructed the vibration isolator designs, they were tested by exciting their base with a random excitation of $0.01 \text{ g}^2 \text{ Hz}^{-1}$ in order to validate the theoretical vibration isolation characteristics. The isolators were mounted on a stiff aluminium base plate bolted to the primary force actuator, i.e., a large electrodynamic shaker. The equipment to be protected from vibrations is represented by a triangular plate at the top of the isolation structure, the mass of which was included in analysis codes by distributing it between three connecting rods.

As can be seen in Fig. 9, the active control element consists of a small shaker mounted in the centre of the base plate and connected to the equipment plate via a 'stinger'. Initial tests were conducted without the active element installed, followed by tests with the active element *in situ*, and finally by tests where the active control was implemented. During these tests, the accelerometers positioned at each of the three equipment plate-to-structure joints measured the vertical acceleration. The transmissibility between the base and equipment could then be calculated. Active control was

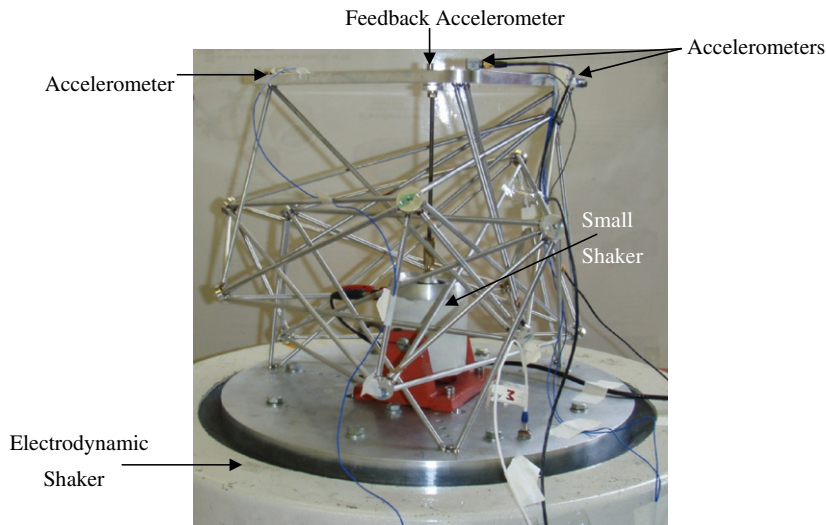


Fig. 9. Experimental set-up for a 5-bay actively controlled, passively optimised structure.

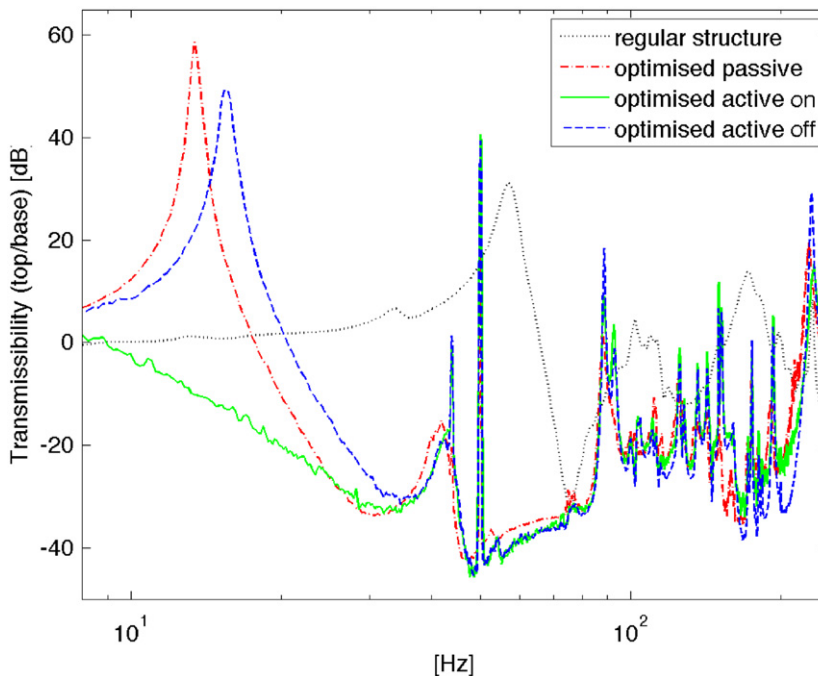


Fig. 10. Plot of experimental equipment average vertical accelerations compared with input base accelerations for 3-bay regular and optimised structures (see Figs. 1 and 2) over the frequency range of 1–250 Hz.

implemented by feeding back the integrated acceleration of the triangular plate, measured using an additional accelerometer at the top of the stinger to the shaker, through a power amplifier.

Both the low-frequency region around the first resonant peak and the higher frequency region of optimisation were studied in detail (although analysis and testing were performed to enable comparison of frequency ranges up to 500 Hz). The results showed that an AVF control system in parallel to a passive isolation structure can attenuate the response at the lowest natural frequency whilst the passive metallic structure controls the response over a specified higher frequency range. The experimental results for the 3-bay irregular structure are plotted in Fig. 10. It can be seen that as expected for this structure, the passively optimised system with AVF control gives the best results.

The optimised structure has a lower stiffness which results in the low frequency (~ 11 Hz) peak appearing in its response compared with a peak at ~ 60 Hz in the non-optimised structure. However, from Fig. 10, it is not immediately

Table 1

Change in transmissibility values for various systems over the frequency band of interest of 150–250 Hz and a slightly wider range of 1–250 Hz. No attempt was made to minimise the weight of the active element.

Structure	Mass ^a (kg)	Integrated transmissibility (dB) 150–250 Hz	Integrated transmissibility (dB) 1–250 Hz
Regular	0.3792	–0.1	–1.3
Optimised passive	0.3224	–13.7	–18.1
Optimised (active element off)	0.3224	–16.7	–19.1
Optimised (active element on)	0.3224	–13.5	–19.3

^a While there will be a mass penalty, the shaker employed in our tests is unrealistically heavy and so their mass figures are omitted. The weight of the joints is also omitted to emphasise the difference in the structures. The overall weight of the optimised structure (with joints as shown in Fig. 3) is 411.4 g.

obvious how effective various systems are and in order to show the effectiveness of the active control system, numbers representing the integrated transmissibility (i.e., areas under the above response curves) are presented in Table 1.

From Table 1, it can be seen that the passive structure has good transmissibility in the frequency range that it has been optimised for (i.e., 150–250 Hz). Furthermore, this optimised irregular structure is about 15% lighter than the regular structure. This is an expected result since in this design the aim is to suppress relatively low frequency modes, which implies that shorter elements would be preferred. This would also mean that the input energy is shifted to the higher end of the vibration spectrum of the structure which may not be desirable. However, based on the results in this design, it is shown that by passively optimising the structure, we are not only incurring any additional weight penalties but even reducing the overall weight of the structure. The active element actually improves the performance over this range even further (when it is turned on). The passively band-optimised structure performs badly over the whole 1–250 Hz range, which is due to the influence of lower resonances.

The best transmissibility figure is for the optimised structure with the active element operating in the 1–250 Hz range. With this configuration, the active element's suppression of the low frequency internal resonant peak (< 150 Hz) is added to the transmissibility reduction achieved by the passively optimised geometry over the frequency range of 150–250 Hz. It should be noted that the numbers in Table 1 represent average transmissibilities and hence the affect of active control is somehow under represented. As can be seen in Fig. 10, the active element has been very successful in suppressing the single resonant peak at around 11 Hz. However, this contribution corresponds to only 1.2 dB average reduction over the frequency range of 150–250 Hz.

6. Conclusions

In this paper, a hybrid GA/SQP optimisation/repair algorithm has been used in the design of a new type of vibration isolator. The isolator was optimised to exploit the reflections that occur as vibrational waves travelling through the structure to provide significant levels of vibration isolation. The absence of viscoelastic elements in such mountings makes the design suitable for use in a vacuum and in high temperature or harsh environments. The essentially undamped passively optimised structure performs well in the frequency range of interest (150–250 Hz) by achieving 13.7 dB reduction in vibration transmissibility. To complement the passive vibration isolation effects, an active system was incorporated by using an electrodynamic shaker with velocity feedback control. This suppresses the response at the fundamental resonance frequency of the system without compromising passive high frequency isolation. This active element, when activated, reduces the transmissibility to 19.3 dB over a wider frequency range of 1–250 Hz. These results indicate of the promise of this new breed of anti-vibration mounting design.

Acknowledgements

This work has been supported by the Engineering and Physical Sciences Research Council: Grant code GR/T19209/01. The authors would like to acknowledge contributions from Drs. Bo Yan and Robin Amy with the experimental work.

References

- [1] C.D. Johnson, Design of passive damping systems, *Journal of Mechanical Design* 117 (B) (1995) 171–176.
- [2] J.F. O'Brien, R. Goullioud, G.W. Neat, Micro-precision interferometer: evaluation of new disturbance isolation solutions, *Proceedings of the International Society for Optical Engineering (SPIE) Conference on Smart Structures and Materials: Passive Damping and Isolation*, San Diego, CA, USA, Vol. 3327, 1998, pp. 387–398.
- [3] R.S. Johal, P.S. Wilke, C.D. Johnson, Satellite component load reduction using SoftRide, *Proceedings of the CSA Engineering, Sixth Responsive Space Conference*, LA, CA, April 28–May 1, 2008.
- [4] R.A. Ibrahim, Recent advances in nonlinear passive vibration isolators, *Journal of Sound and Vibration* 314 (2008) 371–452.
- [5] C.G. Johnson, P.S. Wilke, K.R. Darling, Multi-axis whole-spacecraft vibration isolation for small launch vehicles, *Proceedings of the International Society for Optical Engineering (SPIE) Conference on Smart Structures and Materials: Damping and Isolation*, Newport Beach, CA, USA, Vol. 4331, 2001, pp. 153–161.

- [6] A.J. Keane, A.P. Bright, Passive vibration control via unusual geometries: experiments on model aerospace structures, *Journal of Sound and Vibration* 190 (4) (1996) 713–719.
- [7] M. Moshrefi-Torbati, A.J. Keane, S.J. Elliott, M.J. Brennan, E. Rogers, The integration of advanced active and passive structural noise control methods, *International Journal of Solids and Structures* 43 (2006) 6472–6487.
- [8] K. Shankar, A.J. Keane, Energy flow predictions in a structure of rigidly joined beams using receptance theory, *Journal of Sound and Vibration* 185 (1995) 867–890.
- [9] A.I.J. Forrester, A.J. Keane, Multi-variable geometry repair and optimization of passive vibration isolators, *Third AIAA Multidisciplinary Design Optimization Specialist Conference*, Honolulu, USA, 23–26 April 2007, 10 pp.
- [10] B. Yan, M.J. Brennan, S.J. Elliott, N.S. Ferguson, Active vibration isolation of a system with a distributed parameter isolator using absolute velocity feedback control, *Journal of Sound and Vibration* 329 (10) (2010) 1601–1614.
- [11] A.I.J. Forrester, A.J. Keane, Novel passive vibration isolators, *ISMA International Conference on Noise and Vibration Engineering*, Leuven, Belgium, 2006.
- [12] J. Angeles, C. Truesdell, *Rational Kinematics*, Springer, 1989 (Chapter 6, p. 78 ff, ISBN: 038796813X).
- [13] A. Sobester, Enhancements to Global Design Optimization Techniques, PhD Thesis, University of Southampton, 2003.
- [14] A.I.J. Forrester, A. Sobester, A.J. Keane, *Engineering Design Via Surrogate Modelling—A Practical Guide*, John Wiley & Sons, 2008.
- [15] S.A. Forth, An efficient overloaded implementation of forward mode automatic differentiation in MATLAB, *ACM Transactions on Mathematical Software* 32 (2) (2006) 195–222.
- [16] M. Harrison, A.O. Sykes, M. Martin, Wave effects in isolation mounts, *Journal of the Acoustical Society of America* 24 (1952) 62–71.
- [17] S. Griffin, J. Gussy, S.A. Lane, Virtual skyhook vibration isolation system, *Journal of Vibration and Acoustics: Technical Papers* 124 (1) (2002) 63 (5 pp.).